UCLA
UCLA Electronic Theses and Dissertations

Title
Molecular Dynamics Study of Fragmentation in Protofilaments of Amyloid Beta (16-42)

Permalink
https://escholarship.org/uc/item/88q2w5j1

Author
Tabatabaie-Raissi, Omid

Publication Date
2013

Peer reviewed|Thesis/dissertation

eScholarship.org Powered by the California Digital Library
University of California

UNIVERSITY OF CALIFORNIA

Los Angeles

Molecular Dynamics Study of Fragmentation in Protofilaments of Amyloid Beta (16-42)

A thesis submitted in partial satisfaction of the requirements

for the degree Master of Science in Chemical Engineering

by

Omid Tabatabaie-Raissi

2013

ABSTRACT OF THE THESIS

Molecular Dynamics Study of Fragmentation in Protofilaments of Amyloid Beta (16-42)

by

Omid Tabatabaie-Raissi

Master of Science in Chemical Engineering

University of California, Los Angeles, 2013

Professor Yunfeng Lu, Chair

Through the use of molecular dynamics simulations, we show that fragmentation of Aβ(16-42) protofilaments occurs through the formation of water-conducting glycine vents surrounding the inner pore which then propagate under the increased stress due to C-terminal wrapping. We find that longer protofilaments have an increased propensity to fracture and that the stress-induced propagation of glycine vents is alleviated by thickening of the protofilament to cover exposed hydrophobic residues and reduce C-terminal wrapping. Moreover, we propose that the intrinsic flexibility of glycine-29 in the loop region plays a critical role in the fragmentation of protofilaments. We support this hypothesis by conducting a 1 ns MD simulation on a G29P-mutated 20-mer protofilament. Our results indicate that the increased rigidity of the loop region due to the proline mutation forces the C-terminal to wrap in the opposite direction and therefore prevents the opening of glycine vents, effectively inhibiting fragmentation.

The thesis of Omid Tabatabaie-Raissi is approved.

Selim M. Senkan

Robert F. Hicks

Yunfeng Lu, Chair

University of California, Los Angeles

2013

Table of Contents

Chapter 1. Introduction……1

Chapter 2. Background and Theory

2.1. Protein Folding……..3

2.2 Intrinsically Disordered Proteins and Amyloid Beta…….5

2.3 Molecular Dynamics Simulations……..8

Chapter 3. Methods

3.1 Models……..12

3.2 Simulation Protocol……..16

3.3 Data Analysis……17

Chapter 4. Results and Discussion

4.1 Protofilament Elongation……..19

4.2 Protofilament Thickening……..25

4.3 G29P Mutation……..28

Chapter 5. Conclusion…….31

Appendix…….32

References……...38

Acknowledgements

I would like to thank Dr. Yunfeng Lu and John Berger.

Chapter 1

Introduction

The World Health Organization estimates that there are currently 18 million people worldwide living with Alzheimer's disease (AD). In the United States alone there are roughly 5.2 million people suffering from the disease, with a cost in care of $200 billion in 2013 [1]. According to the Alzheimer's Association, by 2025 the number of people age 65 and older with AD is expected to grow to 7.1 million and by 2050 the social cost of the disease is expected to surpass $1 trillion per year. There is no known cure for AD and its exact cause is unknown.

What is known is that AD is the most common cause of dementia and is characterized by synaptic dysfunction and the loss of neurons. Moreover, AD is associated with the deposition of extra-cellular senile plaques in the grey matter of the brain. The main component of these plaques is the amyloid beta protein, a peptide of 36-43 amino acids whose exact role in the body is not well understood. An increase in the ratio of the 42-residue form of amyloid beta to the more common 40-residue form has been implicated in the early stages of AD [2]. This is due to the fact that the 42-residue form of the protein is more prone to forming the beta-sheet rich amyloid fibers that compose the senile plaques [3]. However, experimental treatments that have removed amyloid plaques from the brain have not been shown to have any effect on dementia [4].



Figure 1.1: Sequence of amyloid beta (1-42). Negatively charged residues are in red, positively charged in blue, polar in green, hydrophobic in black, and glycine in purple

There has been a recent shift in focus from mature fibers to small oligomers as the main neurotoxic species. In fact, studies have shown that amyloid beta oligomers are capable of interacting with cell membranes and disrupting intracellular ion homeostasis [5]. One potential source of these small oligomers is by the fragmentation of fibrillar species of amyloid beta, such as protofilaments or larger fibrils. A protofilament is defined as the smallest fibril-like subunit that can be formed by the aggregation of amyloid beta. Protofilaments can undergo elongation and thickening to form protofibrils, which can then bundle together to form the mature fibers seen in amyloid plaques. Although elongation and thickening are competing mechanisms in the formation of fibers, the elongation of individual protofilaments after a certain size may have a destabilizing effect and lead to fragmentation. Indeed, computer simulations have shown that longer protofilaments have an increased propensity to fracture [6].

Both in vivo and in vitro neurotoxicity studies have implicated amyloid beta oligomers in the range of dimers to nonamers in the pathogenesis of AD [7-8]. Therefore, understanding the mechanism by which these toxic oligomers form is of utmost importance when targeting potential pathways in drug design. In this thesis, we use molecular dynamics (MD) simulations to study the conformational changes of the 16-42 region of the 42-residue amyloid beta protofilament after elongation and thickening, with an emphasis on the mechanism behind fragmentation. In order to do this, we run 1 ns MD simulations on a pentamer, decamer, and 20-mer protofilament, as well as a double-layer 20-mer protofilament with two different stacking interfaces. Moreover, we show that a glycine-29 to proline mutation inhibits the fragmentation of a 20-mer protofilament by increasing the rigidity of the loop region, effectively blocking the formation of glycine vents, and thereby reversing the direction of C-terminal wrapping.

Chapter 2

Background and Theory

2.1 Protein Folding

When a ribosome translates mRNA into a polypeptide during protein synthesis, the nascent chain of amino acids emerges from the exit tunnel in a random coil or unfolded state. This disordered protein must fold into a native three-dimensional structure in order to carry out its desired biological function. It was Anfinsen who postulated that the native fold of a protein in physiological conditions (temperature, pH, ionic concentration, etc.) exists at a unique free energy minimum and is determined only by the protein's amino acid sequence. [9]. However, given the astronomical number of possible conformations for even proteins with modest residue counts, the search for the native state in the conformational space presents a paradox. Put forth by Levinthal in 1969, the paradox arises from the fact that if a protein were to sequentially sample all of its conformations on the path to the native fold, then it would take an inconceivable amount of time for even some of the smallest proteins to fold [10]. For example, a relatively short 40-residue protein containing 39 peptide bonds and 78 phi and psi backbone dihedral angles will have a total of 3^{78} possible conformations (if there are three stable conformations for each bond angle). Therefore, even if each conformation were sampled at a rapid rate of 1 fs^{-1}, it would take 37,000 times longer than the estimated age of the universe for the protein to sample its entire conformational space.

Since proteins have been experimentally observed to fold in seconds or milliseconds, it is logical to assume that there exists a funnel-like free energy landscape that guides the protein from a random coil to its final, functional, three-dimensional structure [11]. This free energy

landscape may be scattered with numerous local free energy minima and on-pathway or off-pathway intermediates and partially folded transition states, but should contain only a single global free energy minimum located at the bottom of the funnel corresponding to the native state. The protein reaches this global free energy minimum by progressively narrowing its conformational entropy through, for example, intra-chain hydrogen bonding, salt bridge formation, and increasing compactness by packing hydrophobic residues into a core and effectively reducing their solvent-accessible surface area [12]. However, it is possible that the native state of the protein may exist in a stable conformation of higher energy if the global free energy minimum is not kinetically accessible [13].

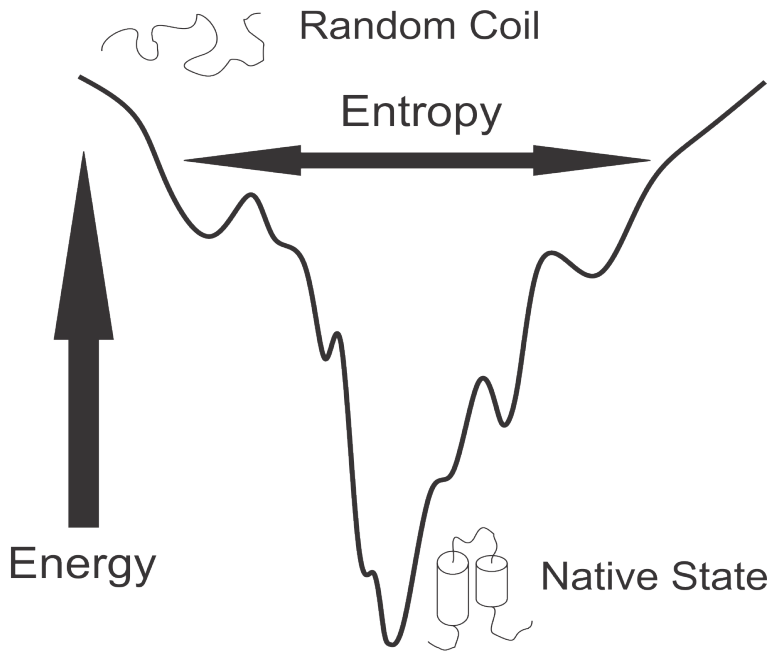


Figure 2.1: The funnel-like free energy landscape

2.2 Intrinsically Disordered Proteins and Amyloid Beta

Intrinsically disordered proteins, or IDP's, serve as an exception to Anfinsen's dogma. Under physiological conditions, IDP's lack an ordered structure and exist as a random coil devoid of the usual packed hydrophobic core characteristic of globular proteins. Although most proteins require a well-defined and folded structure in order to function properly, IDPs constitute a diverse class of proteins whose disordered structure is a requisite for functionality [14]. In fact, it has been estimated that these fully disordered proteins represent 10% of all proteins and that 40% of all eukaryotic proteins contain at least one disordered loop of 50 or more amino acids [15].

The disordered structure of IDP's is involved in a variety of functions. For example, the highly flexible nature of these proteins facilitate in their binding to receptors, ions, or modifying enzymes [16]. The disordered regions of larger proteins can also act as flexible links between domains of the tertiary structure. Moreover, many IDP's can form more ordered structures once they are bound to macromolecules and can even act as molecular switches in the regulation of biological functions [17]. IDP's may also self-aggregate into an overall ordered structure that is energetically stable. Unfortunately, some of these aggregation-prone IDP's form insoluble fibrillar aggregates called amyloids, which are implicated in a number of neurodegenerative diseases such as Alzheimer's, Parkinson's, Huntington's, and Type II Diabetes [18].

One such amyloid forming protein is the 42 residue amyloid beta protein, or Aβ42. Extracellular plaque deposits of Aβ42 in the brain are composed of a network of amyloid fibers and are considered a hallmark of Alzheimer's disease [19]. Early onset of Alzheimer's disease is associated with mutations in either the integral membrane amyloid precursor protein (APP) or

the transmembrane gamma-secretase subunits presenilin-1 or prsenilin-2 (PSEN1, PSEN2) [20]. Depending on where the endoproteolytic cleavage of APP by the proteases beta- and gamma-secretase occurs, 36- to 43-residue peptides of amyloid beta may be released [21]. Although the 40 residue amyloid beta protein, Aβ40, is more abundant, the 42 residue protein, containing two additional hydrophobic residues at the C-terminal, is more fibrillogenic and is the main component of the deposited plaques [22].

Because of their intrinsically disordered nature, Aβ42 monomers exist mainly in a random coil structure with sporadic helical and beta sheet content [23]. However, once they aggregate, Aβ42 monomers are capable of forming a variety of stable oligomer structures, such as pore-forming beta-barrels, amorphous aggregates, and protofilaments [24-26]. The helix-forming protofilament, and subject of this thesis, represents the smallest fibrillar building block that intertwines to form protofibrils, which subsequently bundle into the mature fibers associated with amyloid plaques. Protofilaments of Aβ42 are characterized by a cross-beta structure containing parallel, in-register beta sheets [27]. Within the protofilaments, residues 1-17 constitute a disordered tail that may act as a metal-binding domain, whereas residues 18-25 and 32-42 form antiparallel beta strands perpendicular to the fibril axis and connected by a loop of residues 26-31. The loop region is stabilized by inter-chain salt bridges between Asp23 and Lys28. Although there are several polymorphs of Aβ42 protofilaments, the Luhr's model described above is considered one of the most stable [28].

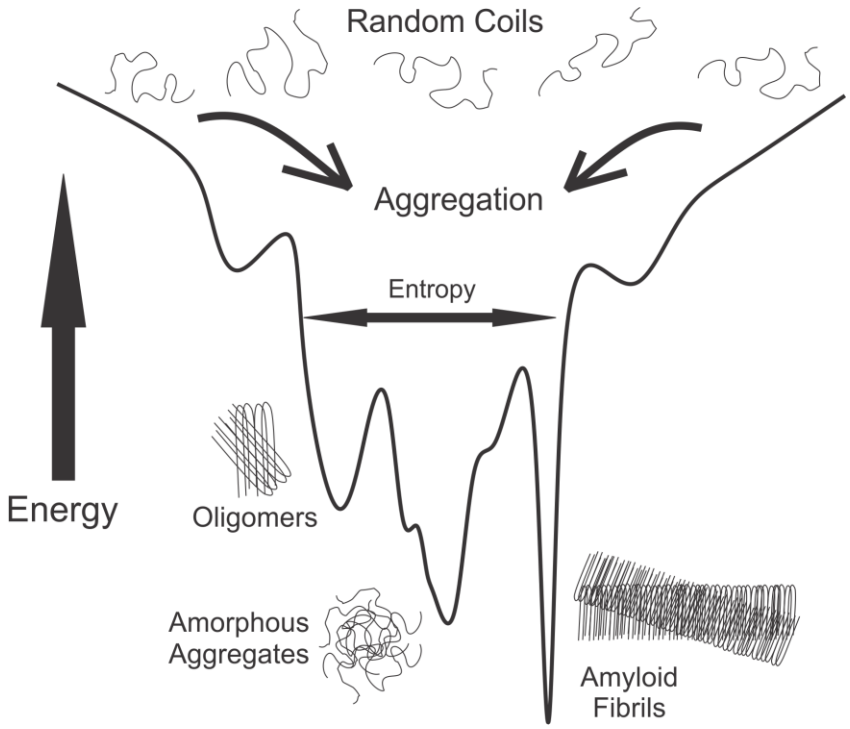


Figure 2.2: Example free energy landscape of Aβ42 during aggregation

Although, initially, it was thought that the insoluble mature amyloid fibers were the toxic species implicated in Alzheimer's disease, there has been a recent shift in focus from mature fibers to soluble oligomers as being the neurotoxic species [29]. In fact, similar levels of amyloid plaque have been found in the brains of many individuals who do not suffer from AD [30]. It has been shown recently that insoluble amyloid fibers may not be entirely nontoxic, but can serve as reservoirs for the more toxic oligomers if fragmented or placed under stress. [31-32]. While the exact mechanism of oligomer-induced toxicity is currently unknown, there is growing evidence that the neurotoxic behavior of fibrillar and prefibrillar oligomers arises from their ability to form pore-like structures or activate ion-regulating receptors such as NMDA; thus, in both cases, disrupting membrane permeability and intracellular ion homeostasis, and eventually resulting in neuronal death [33].

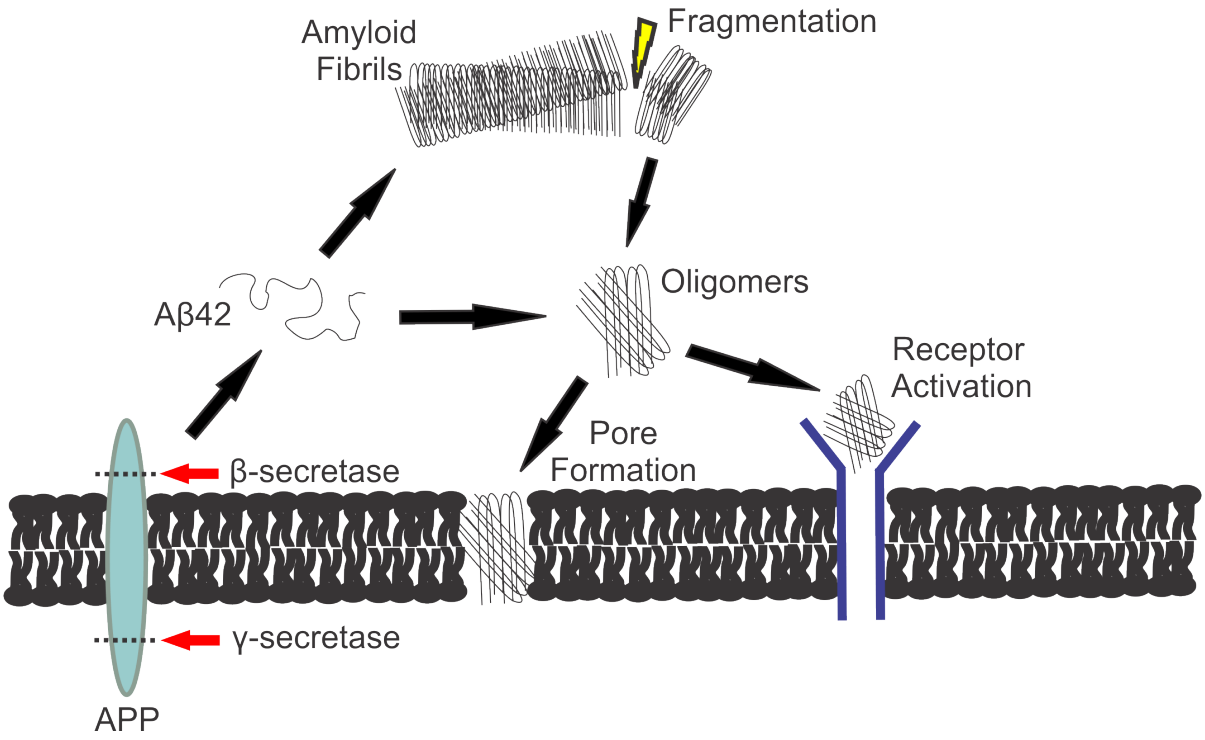


Figure 2.3: Possible pathways to Aβ42 neurotoxicity

2.3 Molecular Dynamics Simulations

Molecular dynamics (MD) simulations serve as a powerful technique for determining the trajectories and thereby various properties for a system of interacting molecules. Because real systems contain a vast amount of atoms, it is not feasible to analytically solve the considerable number of differential equations associated with the equations of motion. However, with the aid of a computer, these equations can be solved numerically, given the initial positions and velocities of each particle as well as an appropriate force field to describe the potential energy. MD simulations allow for the study of dynamic processes in biological systems, including protein folding, substrate docking, ion transport, and membrane interactions. Due to the intensive computational requirements, most MD simulations are limited to the nanosecond timescale. Even

the most powerful supercomputers and distributed computing networks in the world are unable to conduct simulations longer than a small fraction of a second [34].

The simulation software used in this thesis is NAMD, a free and open-source MD program that is developed and maintained by the Theoretical and Computational Biophysics Group at the University of Illinois at Urbana-Champaign [35]. NAMD uses the Verlet leapfrog method of integration to calculate atomic trajectories by the following equations:

$$V_{n+\frac{1}{2}} = V_n + \frac{\Delta t}{2m} F_n \quad (1)$$

$$X_{n+1} = X_n + \Delta t V_{n+\frac{1}{2}} \quad (2)$$

$$F_{n+1} = F(X_{n+1}) \quad (3)$$

$$V_{n+1} = V_{n+\frac{1}{2}} + \frac{\Delta t}{2m} F_{n+1} \quad (4)$$

Where X_n, V_n, and F_n are the position, velocity, and force acting on each atom at timestep n, respectively. The CHARMM27 potential energy function used in NAMD to calculate the force acting on each atom has the form:

$$V = \sum_{bonds} k_b(b - b_0)^2 \quad (5)$$

$$+ \sum_{angles} k_\theta(\theta - \theta_0)^2$$

$$+ \sum_{dihedrals} k_\varphi[1 + \cos(n\varphi - \delta)]$$

$$+ \sum_{impropers} k_\omega(\omega - \omega_0)^2$$

$$+ \sum_{Urey-Bradley} k_u(u - u_0)^2$$

$$+ \sum_{non-bonded} \epsilon[(\frac{R_{min_{ij}}}{r_{ij}}^{12} - \frac{R_{min_{ij}}}{r_{ij}}^{6})] + \frac{q_i q_j}{\epsilon r_{ij}}$$

Where the first 5 summations are the bonded energies described by simple harmonic springs, with the exception of the dihedral bond energy which is described by an angular spring. The last summation contains the non-bonded van der Waals and electrostatic interactions. The spring constants, charges, equilibrium bond distances and angles, and van der Waals constants are all contained in the CHARMM parameter file for proteins, lipids, and nucleic acids. The Urey-Bradley component, an additional potential used to restrain the motion of bonds involved in an angle, has a default value of 0.

In order to simulate biological systems in bulk solvent without worrying about the surface effects induced by a finite simulation cell, periodic boundary conditions (PBC) may be applied to the sides of the box, such that if a molecule were to exit the simulation cell it would reappear inside the cell on the opposite side. For simulations involving solvated proteins, the

dimensions of the periodic boundary cell must be large enough to prevent any undesirable interactions of the protein with its mirror-image.

Four input files are required to run an MD simulation in NAMD. The first is a Protein Data Bank (pdb) file, containing the initial coordinates or positions of each atom in the system. These coordinates are often derived from x-ray crystallography or NMR studies and published in the .pdb format. However, the atomic coordinates alone tell the program nothing about the connectivity between the atoms. This information is found in the Protein Structure File (psf), which explicitly states every bond and bond type. The structure file may be generated by using an appropriate topology file in conjunction with the initial atomic coordinates. The third required input is the CHARMM force field parameter file described previously. Lastly, NAMD requires a user-defined configuration file which contains the simulation protocol: time step, initial velocities (or temperature), number of minimization/equilibration steps, file paths, boundary conditions, restraints, integration parameters, etc. If a file containing the initial atomic velocities is not provided, NAMD can randomly generate a Maxwell-Boltzmann distribution of velocities corresponding to a given temperature. In addition to the four required input files, optional files containing restraints or user-defined forces may also be specified.

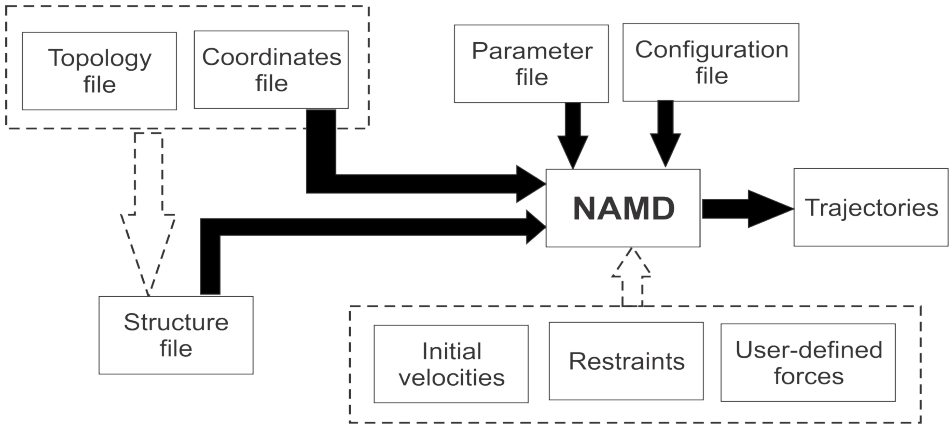


Figure 2.4: NAMD I/O flowchart

Chapter 3

Methods

3.1 Models

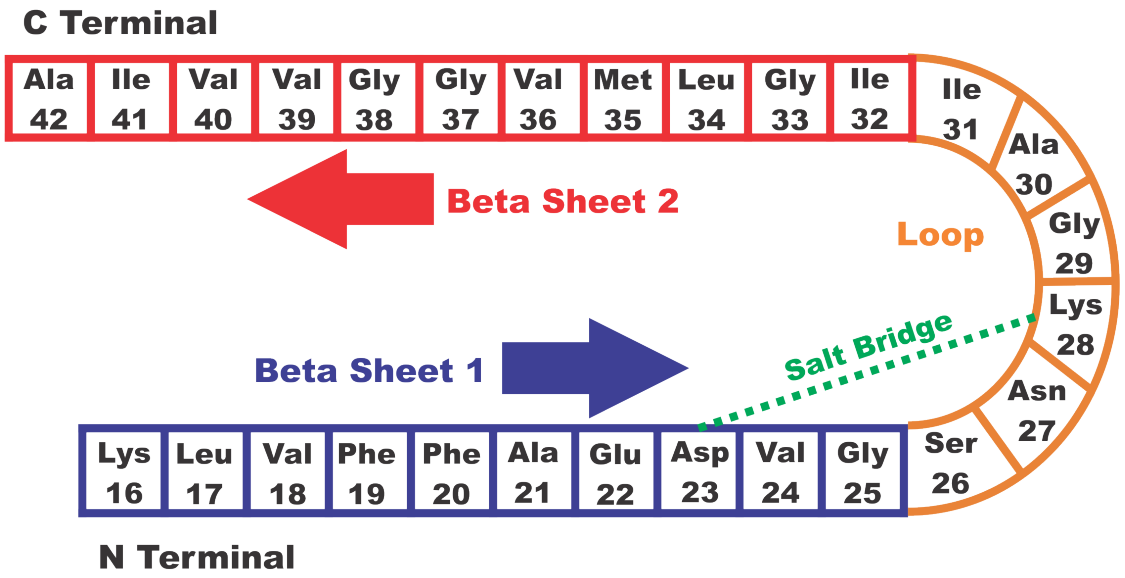


Figure 3.1: Structure of Aβ(16-42) protofilament cross-section in the Luhr's conformation

Molecular dynamics simulations were performed on single- and double- layer Aβ(16-42) models to study the conformational changes of Aβ42 protofilaments after elongation and thickening. Residues 1-15 are excluded from the models as they constitute part of the disordered tail. The structure of the protofilament is based on the Luhr's conformation with the loop region consisting of residues 26-31. Moreover, each protofilament model has a stagger of -1, thus each Lys28 forms a bifurcated salt bridge with Asp23 of the same strand and Asp23 of the previous strand. This staggered structure results in a dangling salt bridge at one end which will be referred to as the "odd end".

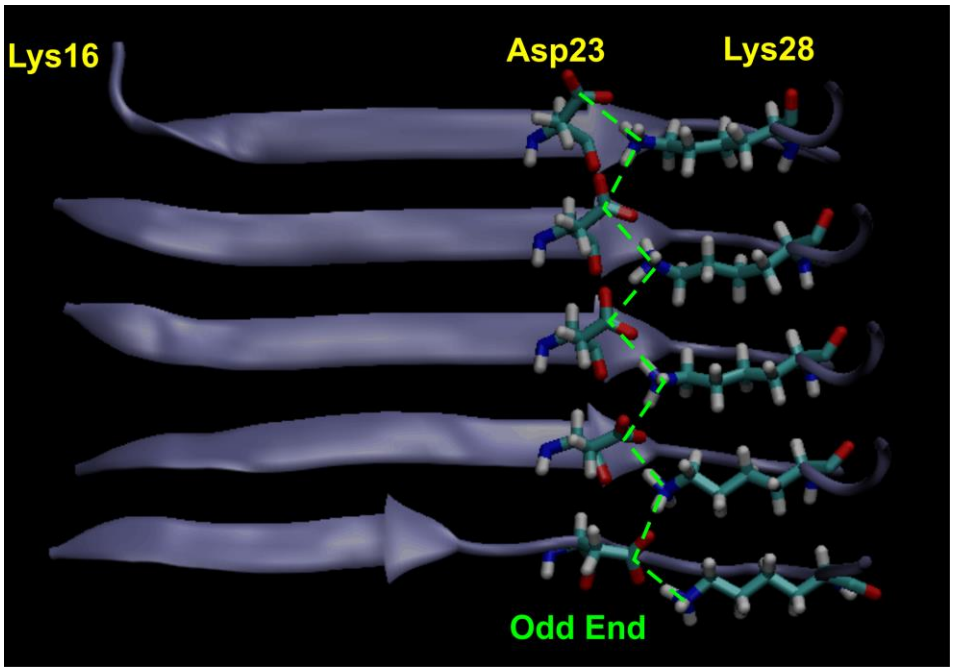


Figure 3.2: View of the staggered salt bridge (only residues 16-30 are shown for clarity)

Single- and double-layer amyloid beta 16-42 protofilament models were constructed from atomic coordinates of amyloid beta 17-42 pentamers derived from hydrogen/deuterium-exchange NMR (PDB code 2BEG) [36]. The coordinates of the third, or central, monomer in the initial pentamer conformation were chosen for repetition in a parallel orientation along the fibril axis to construct the decamer and 20-mer models. The initial spacing between neighboring monomers was 4.8 Å for all models.

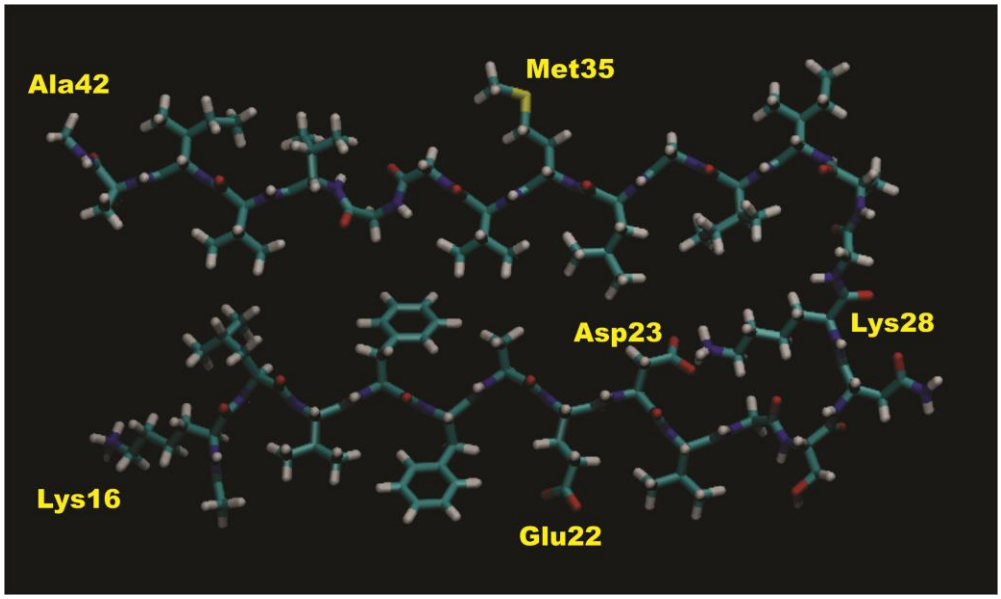


Figure 3.3: All-atom depiction of a protofilament cross-section

For construction of the double-layer protofibril models, two identical decamers, one of which was rotated 180 degrees about the fibril axis, were stacked with a C-terminal to C-terminal (C-C) interface in an antiparallel orientation. The C-C interface was chosen for simulations of protofilament thickening due to the experimental evidence supporting this stacking arrangement in Aβ42 [37]. Protofibril models were constructed for two C-C interfaces: one with an interface consisting of residues 30-42 and another consisting of residues 35-42. The average sheet-to-sheet backbone distance was initially 11.7 Å for the 30-42 (CC) model and 13.4 Å for the 35-42 (CC) model.

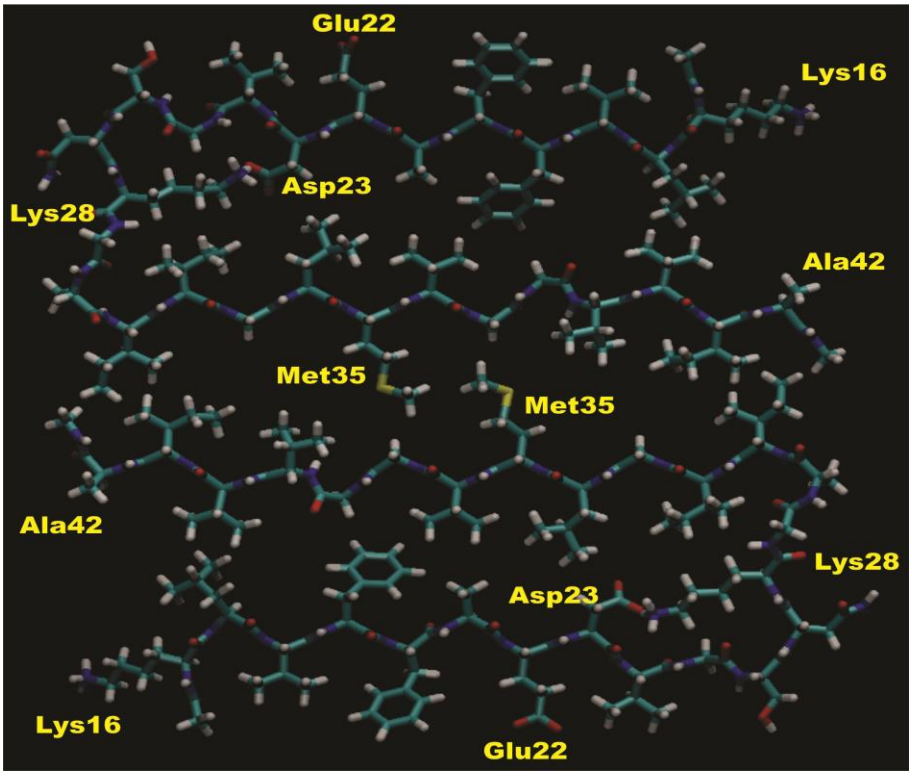


Figure 3.4: All-atom depiction of a double-layer protofilament cross-section with 30-42 (CC) interface

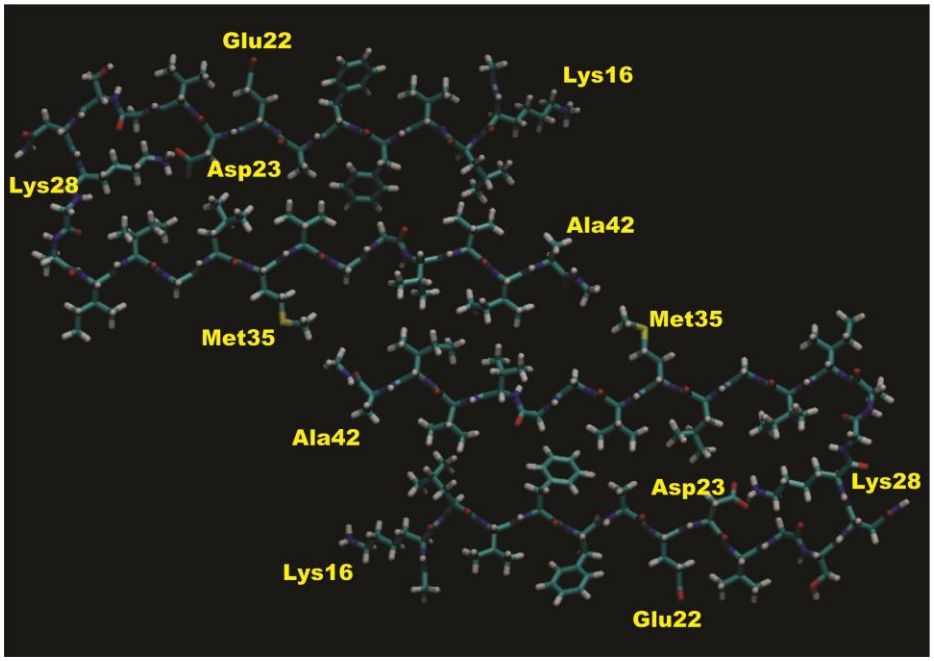


Figure 3.5: All-atom depiction of double-layer protofilament cross-section with 35-42 (CC) interface

In order to neutralize the protein, Lys16 was added to the N-terminal of each monomer for all models using UCSF MODELLER [38], such that each peptide contained an equal number of positively charged residues (Lys16 and Lys28) and negatively charged residues (Glu22 and Asp23). Residue mutations were also created using UCSF MODELLER. Each amyloid beta 16-42 monomer was capped with an acetyl group at the N-terminus and with an N-methyl group at the C-terminus. The protein structure files were generated in VMD using the 'psfgen' plugin with CHARMM27 compatible topology files [37].

3.2 Simulation Protocol

Molecular dynamics simulations were conducted using the NAMD 2.9 program. All simulations were performed in the NPT ensemble using the CHARMM27 force-field in a cubic simulation cell with periodic boundary conditions [40-41]. The temperature was kept constant at 330 K by a Langevin thermostat with a damping coefficient of 1 ps^{-1}. The pressure was maintained at 1 atm using a Berendsen pressure bath coupling with a 100 fs relaxation time. A cut-off of 6.5 Å was used for Van der Waals interactions with a switching distance of 2 Å and a neighbor-list distance of 8 Å. Long-range electrostatic interactions were calculated with the particle mesh Ewald method with a grid spacing of 1 Å [42]. All water molecules were made rigid with the hydrogen-oxygen bond length constrained to its equilibrium value using the SHAKE algorithm [43]. A timestep of 2 fs was used for all simulations.

Single- and double- layer protofilament models were explicitly solvated in a TIP3P water box using the 'solvate' plugin in VMD, with a minimum distance of 10 A between any protein

atom and a side of the box [44-45]. Moreover, any water molecule within 2.5 Å of the protein was removed prior to minimization.

For each simulation, an energy minimization was first carried out on the solvated system for 5000 steps using the conjugate gradient method, with the position of the protein atoms held fixed and the water molecules free to move. An additional 3000 steps of energy minimization were then carried out with all atoms free to move. The system was then equilibrated for 500,000 steps for a total simulation time of 1 ns. Atomic coordinates were printed to output every 250 steps for a total trajectory of 2000 frames. Visualization was performed using VMD [46].

Single-layer models	Total atoms	Protein atoms	Water atoms	Simulation box (Å)	Time (ns)
Pentamer	12681	2025	10656	55 X 50 X 70	1.0
Decamer	20766	4050	16716	90 X 55 X 75	1.0
20mer	33444	8100	25344	135 X 55 X 75	1.0
Double-layer models					
30-42 (CC)	31863	8100	23763	90 X 75 X 80	1.0
35-42 (CC)	41325	8100	33225	90 X 70 X100	1.0

Table 3.1: Simulation details

3.3 Data Analysis

In order to calculate the helix twist of a protofilament, the following equation is used:

$$\theta = \arccos\left(\frac{\boldsymbol{v1} \cdot \boldsymbol{v2}}{|\boldsymbol{v1}| \cdot |\boldsymbol{v2}|}\right) \quad (6)$$

Where **v1** and **v2** are the vectors formed by joining the alpha carbons of residues 18 and 24 on the second and penultimate monomer. The first and last monomers of each chain are excluded

from the calculation to eliminate end-effects. The corresponding angle is then scaled down by 2 for the pentamer, by 7 for the decamer, and by 17 for the 20-mer to obtain the helix twist per monomer. For the double-layer models, the total helix twist was calculated from the average twist of each decamer. Hydrogen bonds were determined for donor-acceptor bond distances less than 3 Å and donor-hydrogen-acceptor angles of less than 20 degrees. Hydrogen bonds were recorded at each frame and scaled down by the number of monomers in each model for comparison.

In order to measure the rate of water diffusion into the hydrated cavity, the number of water molecules within 5 Å of any salt bridge was recorded for each frame of the trajectory. The salt bridges at the ends were excluded to avoid counting water molecules that were within 5 Å of a salt bridge but outside of the pore. Once again the number of water molecules in the pore was scaled down by the number of monomers for comparison. In order to measure the stability of the "odd end", the salt bridge distance was determined for the salt bridge between Asp23 of the first strand and Lys28 of the second. The average "odd end" salt bridge distances for the double-layer models were taken from the average of each decamer. The inter-chain separation was calculated by the average distance between alpha carbons of similar residues on neighboring monomers. The intra-sheet separation was calculated by the average backbone center of mass distances between beta strands of the same monomer. For the double-layer models, the average inter-sheet distance was calculated by the distance between the center of mass of all alpha carbons involved in the corresponding interface. The solvent-accessible surface area was calculated using the "sasa" plugin in VMD by extending each atom's radius by 1.4 Å and determining the points on a sphere that are exposed to solvent. The hydrophobic fraction is defined as the ratio of the solvent-accessible surface area of hydrophobic residues to the total solvent-accessible surface

area. The root mean square deviation (RMSD) of the protein backbone was determined for each simulation using the RMSD trajectory tool in VMD. The minimized initial model was used as the reference. RMSD values were calculated at every other frame, or every 1 ps. For double-layer models, the RMSD values were taken as averages of each protofilament.

Chapter 4

Results and Discussion

4.1 Protofilament Elongation

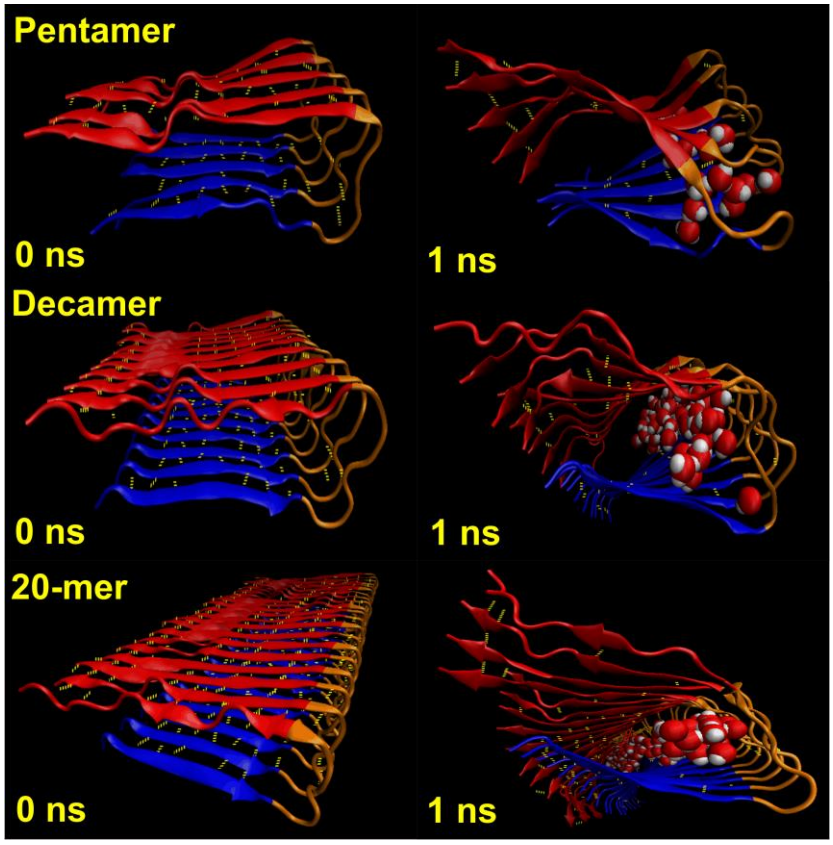


Figure 4.1: Conformational changes of protofilament models before and after 1 ns equilibration

Figure 4.1 shows the initial and final conformation after a 1 ns equilibration for the pentamer, decamer, and 20-mer protofilaments. All three fibrillar oligomers form a left-handed helix during equilibration, consistent with the experimental observation that all biologically-relevant amyloid fibers are left-handed [47]. Starting from an initial twist of 0 degrees prior to energy minimization, both the decamer and 20-mer form helices of roughly 6 degrees per turn after 1 ns, whereas the pentamer forms a highly flexible helix with almost twice the helicity of the longer protofilaments (Figure 4.2A). In addition to the degree of helicity, the increased flexibility of the pentamer can be demonstrated by its greater ability to reduce the hydrophobic fraction of its solvent-accessible surface area through C-terminal wrapping compared to its longer counterparts (Figure 4.2B). This flexible nature of shorter fibrillar oligomers may promote the neurotoxic membrane interactions that are believed to be implicated in AD.

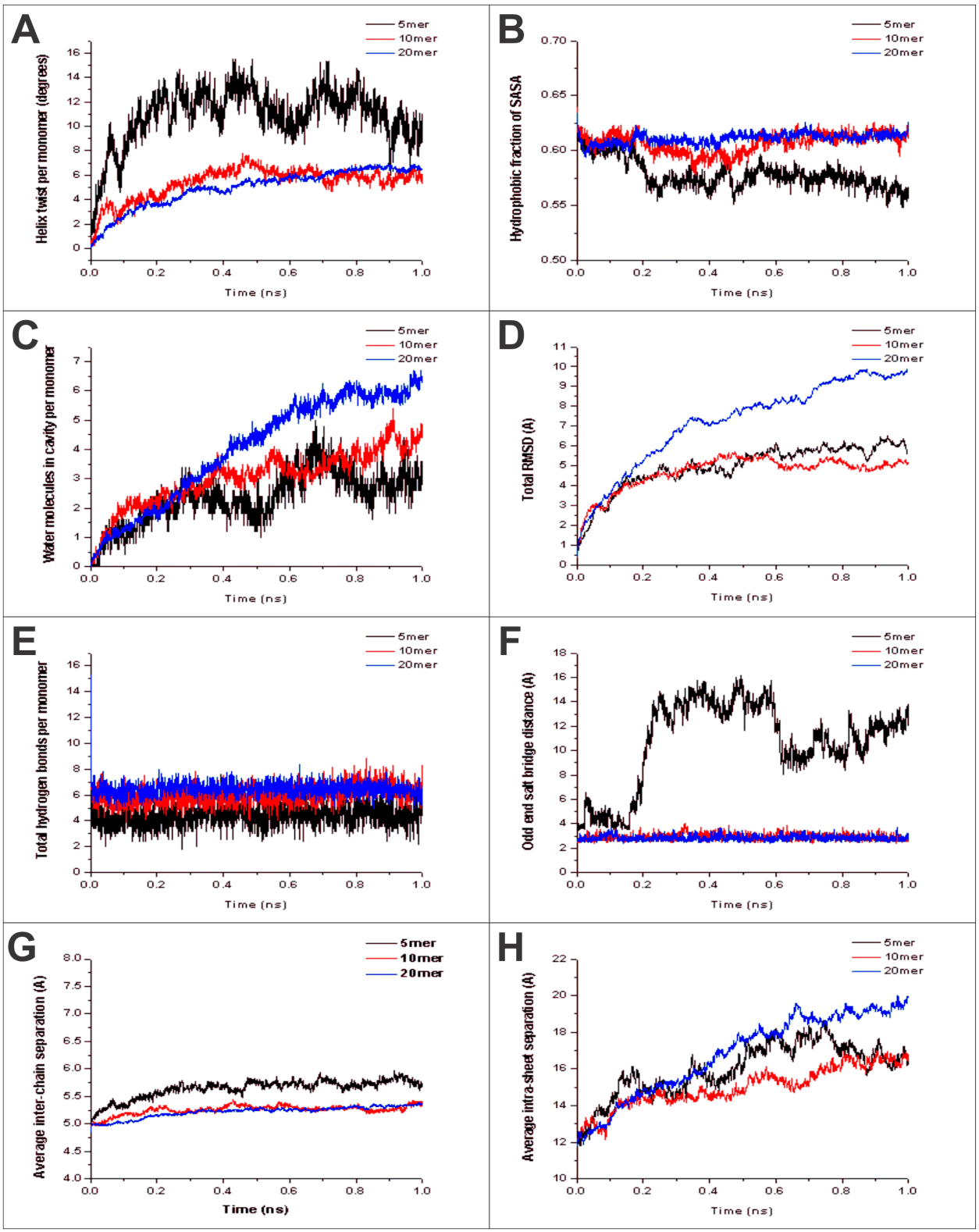


Figure 4.2: Analysis results for protofilament trajectories during 1 ns MD simulation

Over the course of the simulations, all of the protofilament models develop a hydrated inner-pore consisting of a pocket of water molecules surrounded by the side chains of residues 21, 23, 28, 30, 32, and 34. Prior to minimization, any water molecules that may have appeared inside the pore during the initial solvation step are removed so that the diffusion of water into the pore can be studied during the simulation. Although the water molecules mainly tend to enter the pore through the ends of the protofilament, parallel to the fibril axis, we find that water molecules may also breach the inner pore through the loop region and between beta sheets. This perpendicular water conduction originates from the formation of cracks or vents due to the twisting of flexible glycine residues. The increased accommodation of water molecules within the interior of the 20-mer protofilament (Figure 4.2C) is caused by the appearance of large fissures in the N-terminal beta sheet between the 7^{th} and 8^{th} strand and in the C-terminal beta sheet between the 13^{th} and 14^{th} strand (Figure 4.3). These fissures in the 20-mer account for the increase of the RMSD (Figure 4.2D) and intra-sheet separation (Figure 4.2H) compared to the shorter protofilaments. The same type of fissure appears in the C-terminal beta sheet of the decamer between the 6^{th} and 7^{th} strand, however, the propagation of the cracks in the decamer and subsequent disruption of inter-sheet hydrogen bonds is not quite as severe after 1 ns. In the case of the pentamer, a large fissure forms in the loop region between the 1^{st} and 2^{nd} strand that eventually detaches the dangling salt bridge at the odd end.

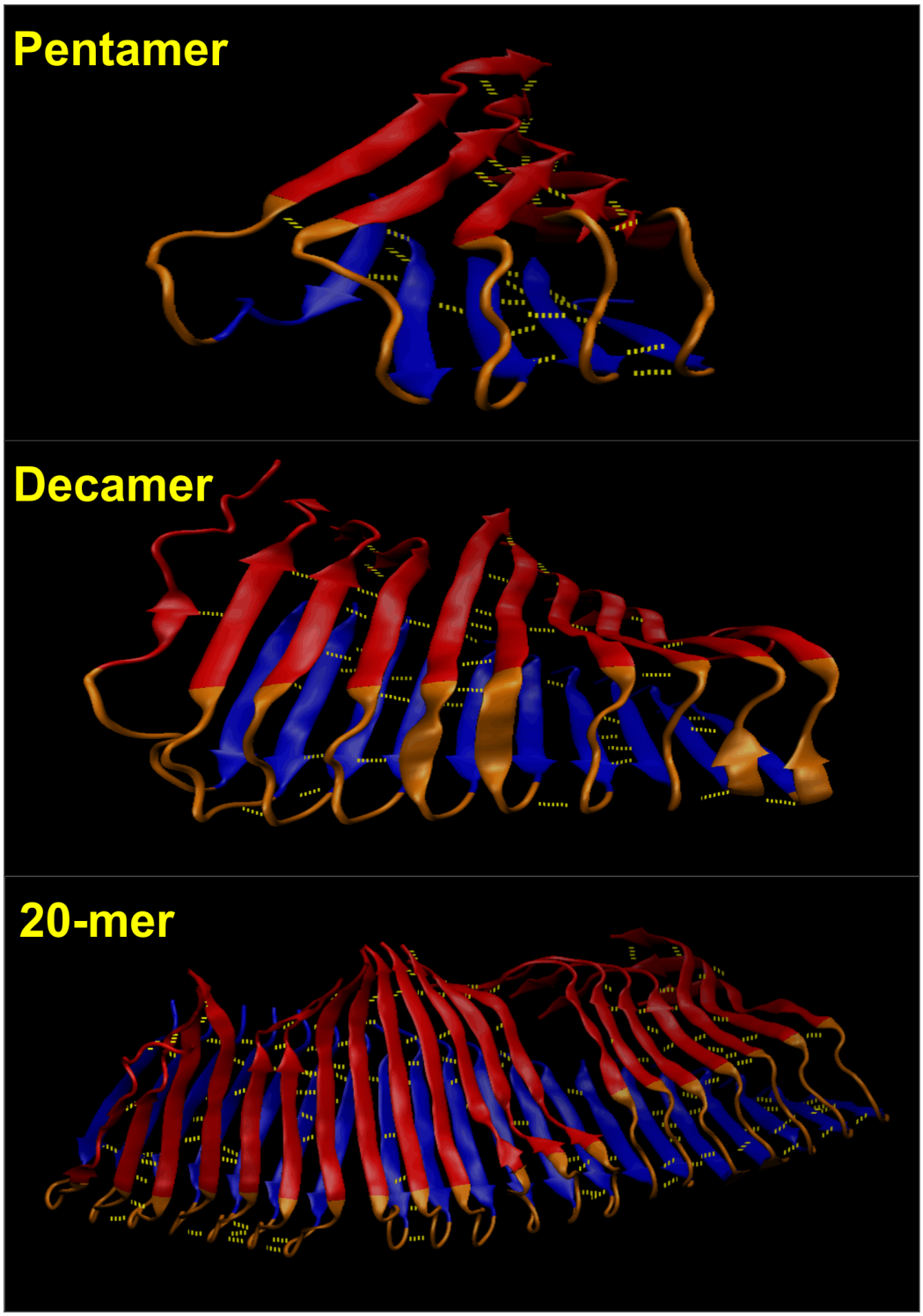


Figure 4.3: Side-view of protofilaments after 1 ns equilibration

From our simulations we find that the formation of these chain-breaking fissures appears to follow a common mechanism. During beta sheet twisting and helix formation, the C-terminal tends to wrap via a Gly37 and Gly38 hinge in order to cover the exposed hydrophobic residues. This wrapping is uneven due to hydrophobic residues at the ends of the protofilament being more exposed. Moreover, the bending of glycine residues disrupts backbone hydrogen bonds and leads to the formation of inter-sheet cracks which can then propagate under increased C-terminal-induced stress, resulting in fractures and, eventually, fragmentation. However, in order for fragmentation to occur, an inter-chain salt bridge must be disconnected, and this requires the propagation of a glycine vent in the loop region. It seems that reducing the flexibility of the loop region will prevent the formation of glycine vents and therefore inhibit protofilament fragmentation.

It is interesting to note the location of the inter-chain breaking points within the protofilament. For example, instead of breaking evenly, the decamer appears to want to break into a tetramer and a hexamer, which happen to be the two most stable pore-forming structures [48-49]. Moreover, the 20-mer appears to fracture into a hexamer and two heptamers, instead of two decamers or two tetramers and two hexamers. This leads us to believe that protofilaments longer than nonamers may have a tendency to form fractures, and eventually fragment, every 6 to 7 strands on average. Indeed, MD simulations on dodecamer protofilaments have shown that they break evenly into two hexamers and simulations on 48-mer protofilaments reveal that they form fractures every 4 to 9 strands [50-51].

4.2 Protofilament Thickening

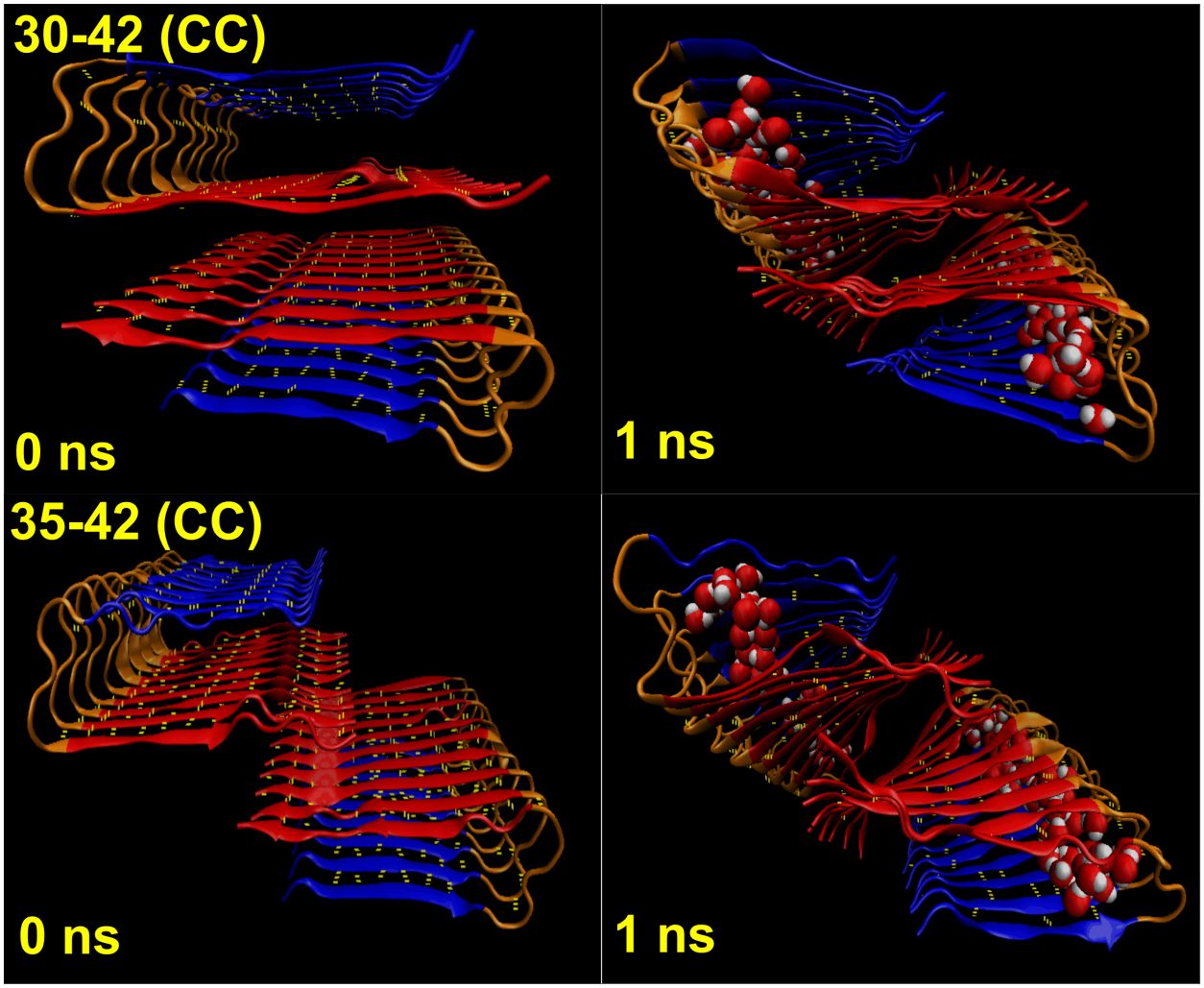


Figure 4.4: Conformational changes of double-layer protofilament models before and after 1 ns equilibration

Figure 4.4 shows the conformation of the double-layer protofilaments before and after a 1 ns equilibration. The reduction in the hydrophobic fraction of solvent-accessible surface area is the main driving force behind protofilament stacking at the C-C interface (Figure 4.5B). This is achieved by forming a steric zipper composed of shape complimentary, hydrophobic residues. A wider steric zipper is formed by stacking at the 30-42 (CC) interface and results in a decreased inter-sheet separation over the 35-42 (CC) interface (Figure 4.6).

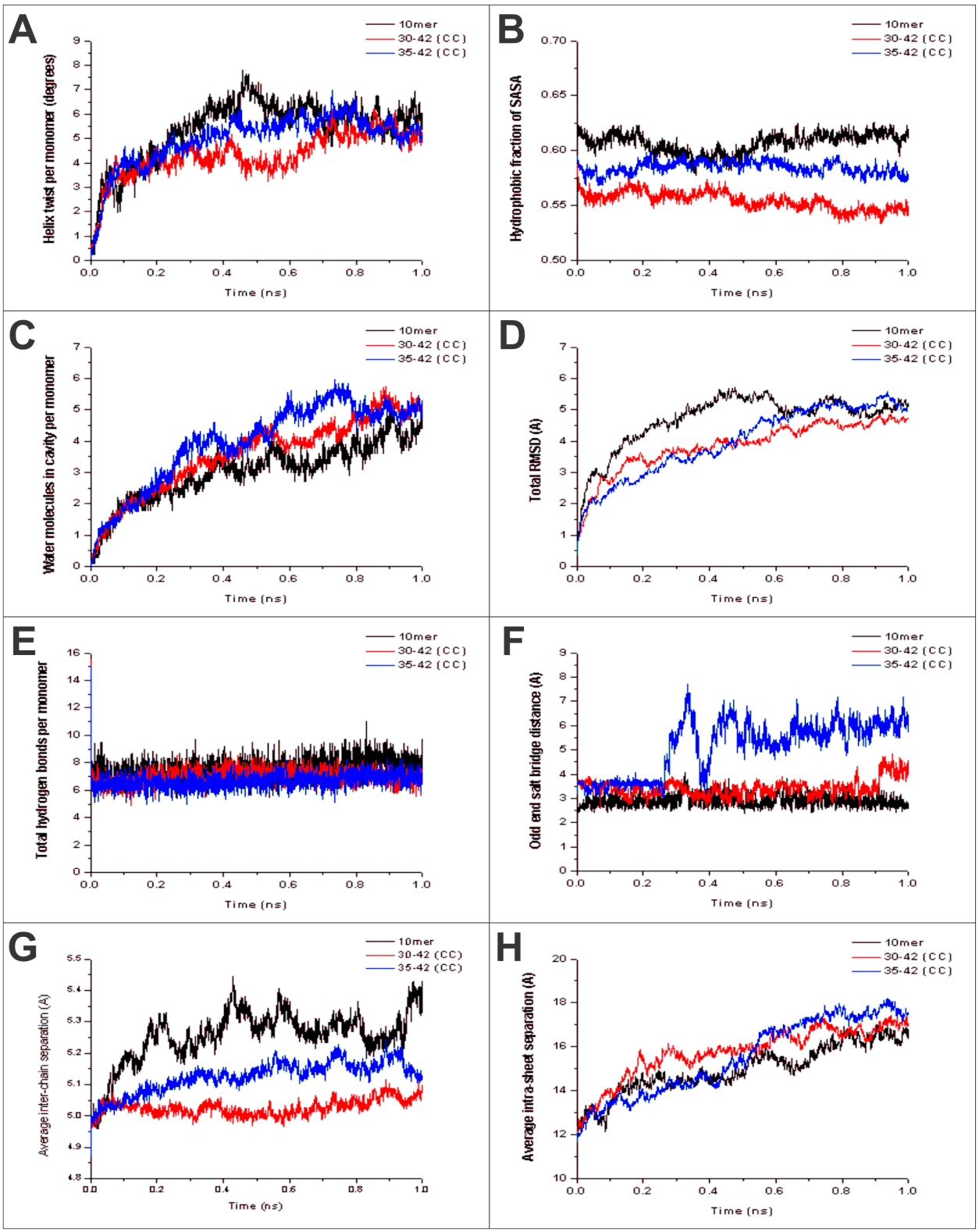


Figure 4.5: Analysis results for double-layer protofilament trajectories during 1 ns MD simulation

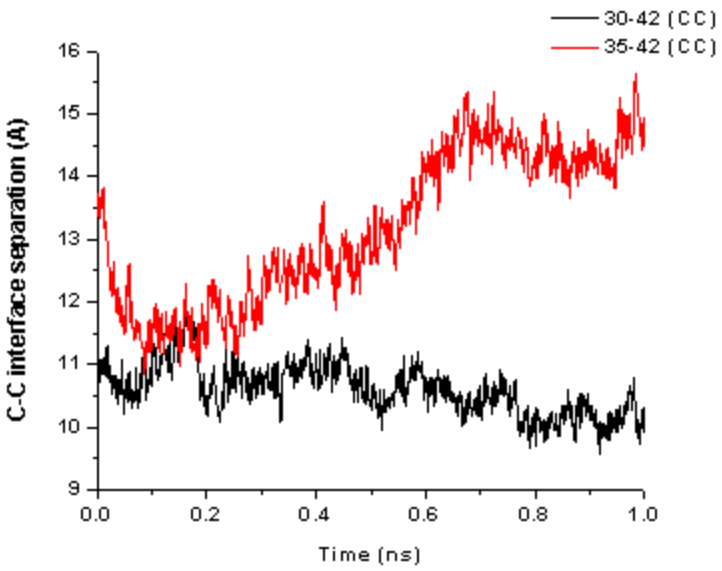


Figure 4.6: Average inter-sheet separation at the C-C interface

More importantly, protofilament thickening does not eliminate the formation of glycine vents surrounding the inner pore or have any significant effect on hydration in the cavity (Figure 4.5C). In fact, the creation of a steric zipper by C-terminal stacking only appears to prevent propagation of these cracks into larger fissures by alleviating the stress induced by C-terminal wrapping and thereby reducing the inter-chain separation (Figure 4.5G). With the exception of the unstable, odd end salt bridge detachment in the 35-42 (CC) model, there are no structurally compromising fractures in the double-layer protofilaments after 1 ns. It has been suggested that the decamer is the turning point in the competition between elongation and thickening and that for protofilaments larger than the decamer thickening is energetically favored over elongation [52]. Therefore, if ten strands is the length at which protofilament fragmentation begins to dominate and if a decamer has a propensity to break into the more stable tetramer and hexamer fragments, it may present a kinetic pathway to the formation of stable and neurotoxic beta-barrel oligomers.

4.3 G29P Mutation

It is believed that the stress caused by the uneven wrapping of the C-terminal to cover exposed hydrophobic residues via the bending of Gly37 and Gly38 causes fragmentation of Aβ42 protofilaments [53]. From our simulations we observe that the onset of chain fracturing is characterized by the formation of glycine vents surrounding the inner pore and that the further propagation of these structural cracks under C-terminal wrapping-induced stress leads to inter-chain salt bridge detachment and eventual protofilament cleavage. However, if this is true then the reverse process must be true as well. In other words, if the inward bending of the C-terminal glycine hinge forces glycine vents to open, then closing these vents should force the C-terminal glycine hinge to bend in the opposite direction. Earlier we had suggested that decreasing the flexibility of the loop region may prevent the formation of glycine vents and thereby inhibit fragmentation. To test this hypothesis we mutate the flexible glycine-29 in the 20-mer model to proline, a rigid residue often found in the loop region of proteins, and run a 1 ns MD simulation.

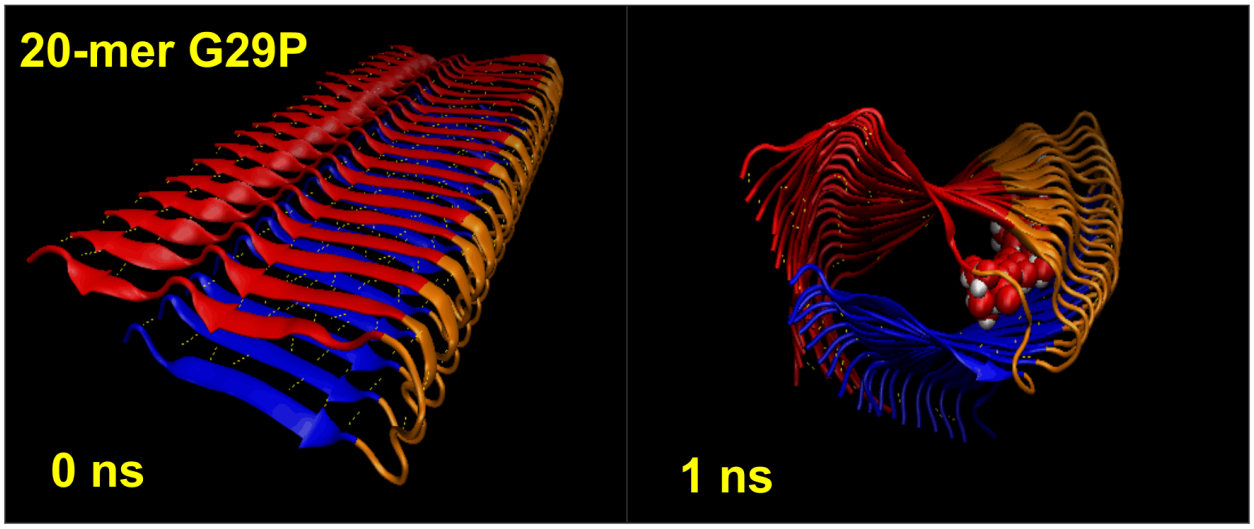


Figure 4.7: Conformational changes of G29P mutated 20-mer before and after 1 ns equilibration

Indeed, the G29P mutant forces a reversal in the direction of bending in the C-terminal glycine hinge (Figure 4.7) and therefore leads to an increase in the hydrophobic fraction of the solvent-accessible surface area compared to the wild type (WT) 20-mer (Figure 4.9B). We find that, with the exception of the odd end strand, the formation of glycine vents is entirely suppressed in the G29P mutated 20-mer after 1 ns and that inner pore water conduction only occurs through the protofilament ends (Figure 4.9C). Moreover, the helix twist in the G29P mutant is reduced by 45% and the RMSD is reduced by 30% compared to the wild type protofilament after 1 ns. Most importantly, other than at the intrinsically unstable odd end strand, there are no inter-chain fractures or structural defects in the G29P mutant (Figure 4.8). The increased rigidity of the loop region in the G29P mutant effectively blocks the formation of glycine vents and results in a tighter inter-chain separation (Figure 4.9G).

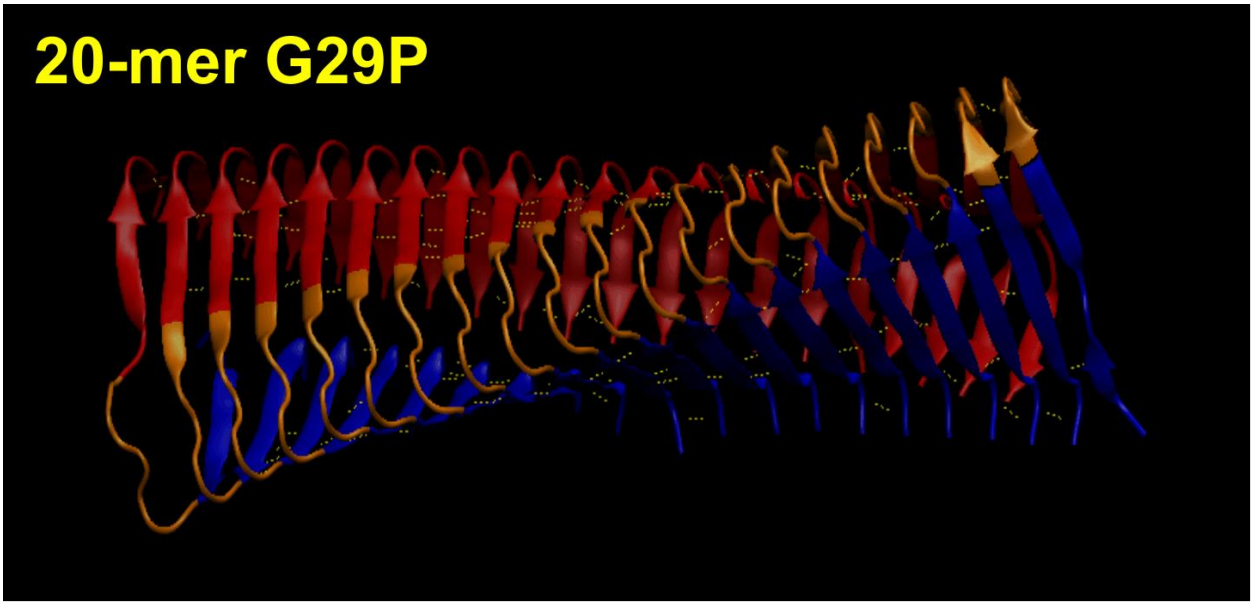


Figure 4.8: Side-view of G29P mutated 20-mer after 1 ns equilibration

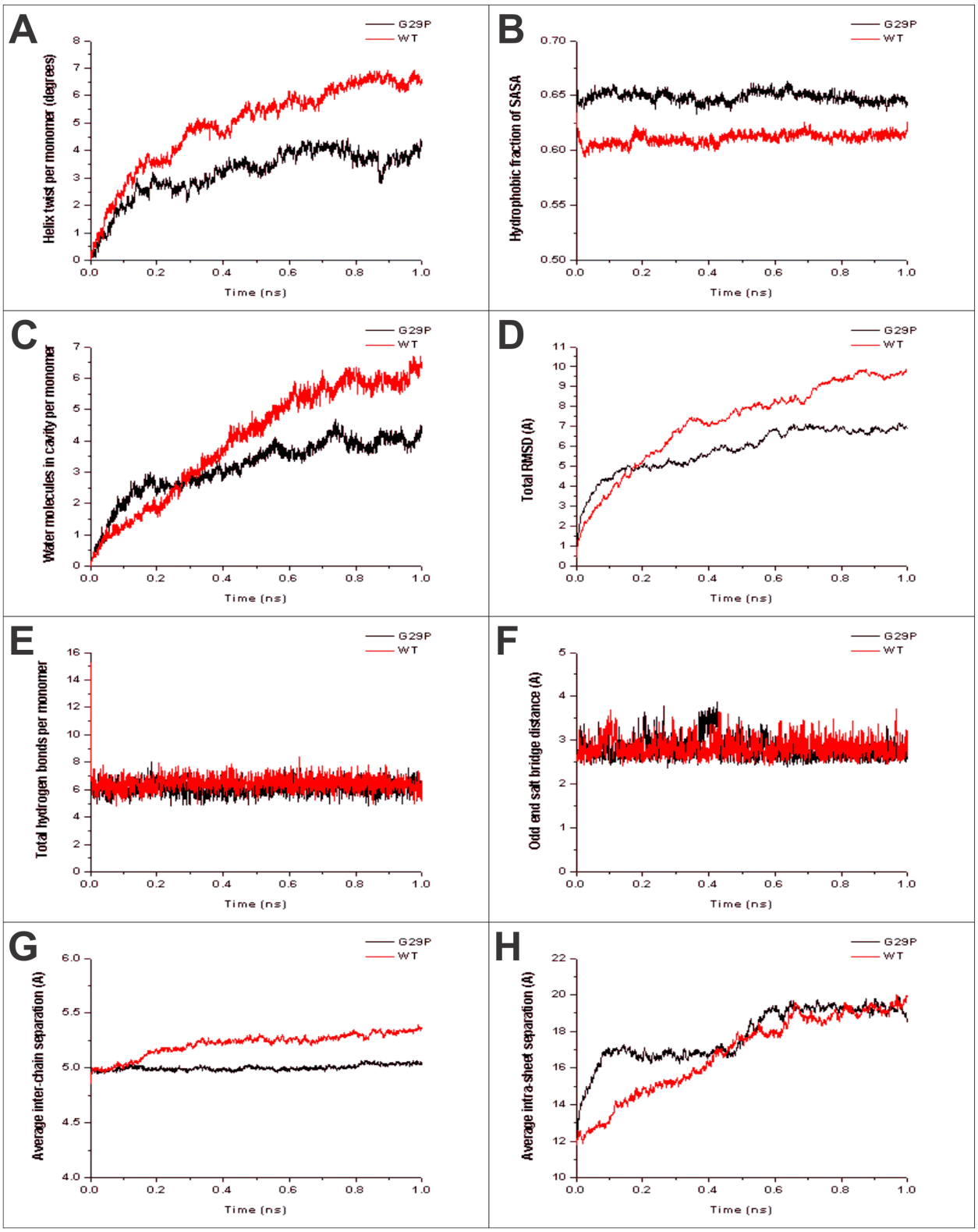


Figure 4.9: Analysis results of G29P mutated 20-mer trajectories during 1 ns MD simulation

Chapter 5

Conclusion

Through the use of short molecular dynamics simulations, we have shown that fragmentation of Aβ42 protofilaments occurs through the formation of water-conducting glycine vents surrounding the inner pore which then propagate under the increased stress due to C-terminal wrapping. We find that longer protofilaments have an increased propensity to fracture and that the stress-induced propagation of glycine vents is alleviated by thickening of the protofilament to cover exposed hydrophobic residues and reduce C-terminal wrapping. Moreover, we propose that the intrinsic flexibility of glycine-29 in the loop region plays a critical role in the fragmentation of protofilaments. We support this hypothesis by conducting a 1 ns MD simulation on a G29P-mutated 20-mer protofilament. Our results show that the increased rigidity of the loop region due to the proline mutation forces the C-terminal to wrap in the opposite direction and therefore prevents the opening of glycine vents, effectively inhibiting fragmentation.

Although the underlying mechanism behind aggregation and oligomer formation remains unknown, it is apparent that in order to form the insoluble amyloid fibrils associated with Alzheimer's disease, Aβ42 monomers must eventually pass through the stage of protofilament elongation and thickening. Furthermore, as these fibrillar oligomers are susceptible to fragmentation, they may serve as a source for additional nucleation seeds or even more toxic oligomers. Therefore, controlling the kinetics of protofilament fragmentation presents a potential path to reducing neurotoxicity in Alzheimer's disease by promoting the formation of less toxic species and perhaps along the way gaining some insight into similar amyloidogenic diseases.

Appendix

A. Average values for the final 0.2 ns of simulation (Standard deviation in parenthesis)

	Pentamer	Decamer	20mer	G29P	30-42 (CC)	35-42 (CC)
Helix twist per monomer (degrees)	10.53 (1.55)	5.80 (0.40)	6.56 (0.16)	3.70 (0.28)	5.29 (0.34)	5.38 (0.30)
Water molecules in cavity per monomer	2.82 (0.43)	4.14 (0.39)	5.97 (0.25)	3.98 (0.20)	5.00 (0.28)	4.93 (0.19)
Hydrophobic fraction of SASA	0.57 (0.01)	0.61 (0.01)	0.61 (0.01)	0.65 (0.01)	0.55 (0.01)	0.58 (0.01)
Odd end salt bridge distance (Å)	11.45 (1.09)	2.85 (0.23)	2.82 (0.21)	2.70 (0.14)	3.76 (0.48)	5.97 (0.39)
Average Intra-sheet distance (Å)	16.69 (0.45)	16.46 (0.24)	19.26 (0.26)	19.24 (0.23)	16.85 (0.29)	17.57 (0.25)
C-C inter-sheet distance (Å)	-	-	-	-	10.14 (0.20)	14.41 (0.35)
Total RMSD (Å)	5.97 (0.27)	5.01 (0.15)	9.59 (0.14)	6.83 (0.13)	4.61 (0.12)	5.17 (0.16)
Beta sheet 1 RMSD (Å)	3.35 (0.24)	2.99 (0.23)	6.28 (0.28)	3.77 (0.18)	2.75 (0.13)	3.06 (0.17)
Loop RMSD (Å)	3.49 (0.31)	2.24 (0.24)	6.32 (0.31)	2.77 (0.12)	2.29 (0.07)	2.64 (0.15)
Beta sheet 2 RMSD (Å)	3.80 (0.30)	4.36 (0.20)	7.09 (0.26)	5.56 (0.11)	2.91 (0.10)	3.59 (0.11)
Total inter-chain separation (Å)	5.76 (0.07)	5.28 (0.06)	5.32 (0.03)	5.04 (0.01)	5.06 (0.02)	5.16 (0.03)
Beta sheet 1 inter-chain separation (Å)	5.83 (0.08)	4.96 (0.03)	5.08 (0.02)	5.05 (0.02)	5.07 (0.03)	5.13 (0.03)
Loop inter-chain separation (Å)	6.88 (0.17)	5.27 (0.09)	5.51 (0.03)	5.16 (0.03)	5.23 (0.05)	5.47 (0.06)
Beta sheet 2 inter-chain separation (Å)	5.09 (0.05)	5.59 (0.10)	5.45 (0.06)	4.96 (0.02)	4.95 (0.02)	5.02 (0.02)
Total hydrogen bonds per monomer	4.58 (0.86)	6.55 (0.67)	6.39 (0.49)	6.22 (0.49)	6.92 (0.47)	7.02 (0.47)
Beta sheet 1 hydrogen bonds per monomer	1.73 (0.54)	2.90 (0.46)	2.78 (0.33)	2.35 (0.29)	2.58 (0.30)	2.81 (0.29)
Loop hydrogen bonds per monomer	0.41 (0.25)	0.74 (0.22)	0.77 (0.17)	0.80 (0.17)	0.74 (0.15)	0.77 (0.15)
Beta sheet 2 hydrogen bonds per monomer	2.32 (0.56)	2.78 (0.45)	2.69 (0.29)	2.77 (0.32)	3.41 (0.32)	3.25 (0.33)

B. Tcl analysis script for 20-mer protofilament

```
###  Helix twist  ###

#set s1 to second strand
set s1 P2
#set s2 to penultimate strand
set s2 P19
#open file for writing
set output [open twist w]
#set range for trajectory (frame 32 is after minimization)
for {set i 32} {$i <= 2032} {incr i} {
#select alpha carbons for resid 18 and 24 on second strand
     set c18 [atomselect top "protein and segid $s1 and resid 18 and
name CA" frame $i]
     set c24 [atomselect top "protein and segid $s1 and resid 24 and
name CA" frame $i]
#create vector connecting alpha carbons on second strand
     set v18 [lindex [$c18 get {x y z}] 0]
     set v24 [lindex [$c24 get {x y z}] 0]
     set v1 [vecsub $v24 $v18]
#delete selections to prevent memory leaks
     $c18 delete
     $c24 delete
#repeat for penultimate strand
     set c18 [atomselect top "protein and segid $s2 and resid 18 and
name CA" frame $i]
     set c24 [atomselect top "protein and segid $s2 and resid 24 and
name CA" frame $i]
     set v18 [lindex [$c18 get {x y z}] 0]
     set v24 [lindex [$c24 get {x y z}] 0]
     set v2 [vecsub $v24 $v18]
     $c18 delete
     $c24 delete
     set vl1 [veclength $v1]
     set vl2 [veclength $v2]
#calculate twist angle from eq. (6) and scale by 17
     set denom [expr $vl1 * $vl2]
     set dot [vecdot $v1 $v2]
     set twist [expr 57.296*acos($dot / $denom) / 17.0 ]
#calculate time from frame and timestep
     set time [expr ($i-32)/2.0]
#output time and twist angle
     puts $output "$i $twist"
}
#close file
close $output
```

```
###  Pore hydration  ###

set output [open pore w]
for {set i 32} {$i <= 2032} {incr i} {
     set time [expr ($i-32)/2.0]
#select water molecules within 5 A of delta carbon on lys28 or 5 #A of
gamma carbon on asp23 ande exclude end strands and select #oxygens to
prevent double counting of hydrogens
     set num [atomselect top "element O and water {within 5 of name CD
and resid 28 and not segid P1 and not segid P20} or {within 5 of name
CG and resid 23 and not segid P1 and not segid P20}" frame $i]
#count number of water molecules and print to file
     set res [$num get resid]
     set numwater [llength $res]
     puts $output "$time $numwater"
     $num delete
}
close $output

### Hydrogen bonds ###

#select residue regions for counting hydrogen bonds
set beta1 [atomselect top "protein and backbone and resid 16 to 25"]
set beta2 [atomselect top "protein and backbone and resid 32 to 42"]
set all [atomselect top "protein and backbone"]
set loop [atomselect top "protein and backbone and resid 26 to 31"]
#use VMD hbonds plugin to count hbonds
#for default D-A distance of 3 A and D-H-A angle <20 degrees
hbonds -sel1 $beta1 -frames 32:2032 -plot no -writefile yes -outfile
hbonds_beta1.dat
hbonds -sel1 $beta2 -frames 32:2032 -plot no -writefile yes -outfile
hbonds_beta2.dat
hbonds -sel1 $all -frames 32:2032 -plot no -writefile yes -outfile
hbonds_all.dat
hbonds -sel1 $loop -frames 32:2032 -plot no -writefile yes -outfile
hbonds_loop.dat
$beta1 delete
$beta2 delete
$all delete
$loop delete


### Inter-chain separation ###

#set protofilament length
set chain 20
#calculate number of alpha carbon pairs for each region to obtain
#averages later
set total [expr (($chain - 1) * 27)]
set beta1 [expr (($chain - 1) * 10)]
set loop [expr (($chain - 1) * 6)]
set beta2 [expr (($chain - 1) * 11)]
```

```
set output [open chainsep w]
for {set i 32} {$i <= 2032} {incr i} {
#intialize region sums to zero
     set beta1sum 0
     set loopsum 0
     set beta2sum 0
#set strand range to j-1 pairs of alpha carbons
     for {set j 1} {$j < $chain} {incr j} {
#set resid range to beta sheet 1
          for {set k 16} {$k <= 25} {incr k} {
#select alpha carbon of resid k and strand j
                set ca1 [atomselect top "name CA and resid $k and
segid P${j}" frame $i]
#set jplus to adjacent strand
                set jplus [expr ($j+1)]
#select alpha carbon of resid k and strand j+1
                set ca2 [atomselect top "name CA and resid $k and
segid P${jplus}" frame $i]
#calculate distance between alpha carbons
                set vca1 [lindex [$ca1 get {x y z}] 0]
                set vca2 [lindex [$ca2 get {x y z}] 0]
                set dist [vecdist $vca1 $vca2]
#add distances to sum counter
                set beta1sum [expr ($beta1sum + $dist)]
                $ca1 delete
                $ca2 delete
          }
#repeat for loop region
          for {set k 26} {$k <= 31} {incr k} {
                set ca1 [atomselect top "name CA and resid $k and
segid P${j}" frame $i]
                set jplus [expr ($j+1)]
                set ca2 [atomselect top "name CA and resid $k and
segid P${jplus}" frame $i]
                set vca1 [lindex [$ca1 get {x y z}] 0]
                set vca2 [lindex [$ca2 get {x y z}] 0]
                set dist [vecdist $vca1 $vca2]
                set loopsum [expr ($loopsum + $dist)]
                $ca1 delete
                $ca2 delete
          }
#repeat for beta sheet 2
          for {set k 32} {$k <= 42} {incr k} {
                set ca1 [atomselect top "name CA and resid $k and
segid P${j}" frame $i]
                set jplus [expr ($j+1)]
                set ca2 [atomselect top "name CA and resid $k and
segid P${jplus}" frame $i]
                set vca1 [lindex [$ca1 get {x y z}] 0]
                set vca2 [lindex [$ca2 get {x y z}] 0]
                set dist [vecdist $vca1 $vca2]
                set beta2sum [expr ($beta2sum + $dist)]
```

```
                $ca1 delete
                $ca2 delete
            }
        }
#calculate time from frame and timestep
        set time [expr ($i-32)/2.0]
#calculate total sum of all adjacent alpha carbon distances
        set totalsum [expr ($beta1sum + $loopsum + $beta2sum)]
#scale each sum by total number of pairs per region
        set beta1sep [expr ($beta1sum / $beta1)]
        set loopsep [expr ($loopsum / $loop)]
        set beta2sep [expr ($beta2sum / $beta2)]
#scale total sum by total pairs to calculate average
        set totalsep [expr ($totalsum / $total)]
#print average inter-chain distance for each region and total
        puts $output "time $time beta1 $beta1sep loop $loopsep beta2
$beta2sep total $totalsep"
}
close $output


### Intra-sheet separation ###


set output [open ncsep w]
for {set i 32} {$i <= 2032} {incr i} {
#initialize sum to zero
        set sum 0
#set the range to the number of monomers set previously
        for {set j 1} {$j <= $chain} {incr j} {
#select alpha carbons in beta strand 1
                set ca1 [atomselect top "name CA and resid 16 to 25
and segid P${j}" frame $i]
#select alpha carbons in beta strand 2
                set ca2 [atomselect top "name CA and resid 32 to 42
and segid P${j}" frame $i]
#measure the center of mass of both strands
                set com1 [measure center $ca1 weight mass]
                set com2 [measure center $ca2 weight mass]
#measure distance between center of masses
                set dist [vecdist $com1 $com2]
#add to sum counter
                set sum [expr ($sum + $dist)]
                $ca1 delete
                $ca2 delete
            }
        set time [expr ($i-32)/2.0]
#scale total distances by number of monomers to get average
        set ncsep [expr ($sum / $chain)]
#print time and average intra-sheet separation to file
        puts $output "$time $ncsep"
}
```

```
close $output


### Hydrophobic SASA ###

set output [open sasa w]
for {set i 32} {$i <= 2032} {incr i} {
     set time [expr ($i-32)/2.0]
#select all protein residues
     set prot [atomselect top "protein" frame $i]
#select hydrophobic residues
     set hydro [atomselect top "protein and hydrophobic" frame $i]
#use VMD sasa plugin to measure solvent accessible surface #area
     set tsasa [measure sasa 1.4 $prot]
#repeat and restrict surface area to hydrophobic residues
     set hsasa [measure sasa 1.4 $prot -restrict $hydro]
#calculate hydrophobic fraction of SASA
     set sasafrac [expr ($hsasa / $tsasa)]
#print time and hydrophobic fraction to file
     puts $output "$time $sasafrac"
     $prot delete
     $hydro delete
}
close $output
```

References

[1] Alzheimer's Association. www.alz.org.

[2] Riek, Roland, et al. "NMR studies in aqueous solution fail to identify significant conformational differences between the monomeric forms of two Alzheimer peptides with widely different plaque-competence, Aβ (1–40) ox and Aβ (1–42) ox." *European Journal of Biochemistry* 268.22 (2001): 5930-5936.

[3] Findeis, Mark A. "The role of amyloid β peptide 42 in Alzheimer's disease."*Pharmacology & therapeutics* 116.2 (2007): 266-286.

[4] Holmes C. Long-term Effects of Abeta42 Immunisation in Alzheimer's Disease: Follow-up of a Randomised, Placebo-controlled Phase I Trial. *Lancet*. 2008;372(9634):216–23.

[5] Aisenbrey, Christopher, et al. "How is protein aggregation in amyloidogenic diseases modulated by biological membranes?." *European Biophysics Journal*37.3 (2008): 247-255.

[6] Kahler A, Sticht H, Horn AHC (2013) Conformational Stability of Fibrillar Amyloid-Beta Oligomers via Protofilament Pair Formation – A Systematic Computational Study. PLoS ONE 8(7): e70521.

[7] Gong, Yuesong, et al. "Alzheimer's disease-affected brain: presence of oligomeric Aβ ligands (ADDLs) suggests a molecular basis for reversible memory loss." *Proceedings of the National Academy of Sciences* 100.18 (2003): 10417-10422.

[8] Bernstein SL, Dupuis NF, Lazo ND, Wyttenbach T, Condron MM, et al. Amyloid-b protein oligomerization and the importance of tetramers and dodecamers in the aetiology of Alzheimer's disease. Nature Chemistry: 1: (2009): 326– 331.

[9] Anfinsen, Christian B. "Studies on the principles that govern the folding of protein chains." (1972).

[10] Levinthal, Cyrus. "How to fold graciously." *Mossbauer spectroscopy in biological systems* (1969): 22-24.

[11] Zwanzig, Robert, Attila Szabo, and Biman Bagchi. "Levinthal's paradox."*Proceedings of the National Academy of Sciences* 89.1 (1992): 20-22.

[12] Dill, Ken A., and Hue Sun Chan. "From Levinthal to pathways to funnels."*Nature structural biology* 4.1 (1997): 10-19.

[13] Hunter, Philip. "Into the fold." *EMBO reports* 7.3 (2006): 249.

[14] Wright PE, Dyson HJ. Intrinsically unstructured proteins: re-assessing the protein structure-function paradigm. J Mol Biol. 1999 Oct 22;293(2):321-31.

[15] Tompa P. Intrinsically unstructured proteins. Trends Biochem Sci. 2002 Oct;27(10):527-33.

[16] Collins, Mark O., et al. "Phosphoproteomic analysis of the mouse brain cytosol reveals a predominance of protein phosphorylation in regions of intrinsic sequence disorder." *Molecular & Cellular Proteomics* 7.7 (2008): 1331-1348.

[17] Sandhu KS, Dash D. "Dynamic alpha-helices: conformations that do not conform".*Proteins* 68 (1): (2007) 109–22.

[18] Selkoe, Dennis J. "Folding proteins in fatal ways." *Nature* 426.6968 (2003): 900-904.

[19] Parker MH, Reitz A.B. "Assembly of β-Amyloid Aggregates at the Molecular Level". *Chemtracts-Organic Chemistry* 13(1): (200): 51–56.

[20] Murphy, M. Paul, and Harry LeVine, III. "Alzheimer's Disease and the Amyloid-β Peptide." *Journal of Alzheimer's Disease* 19.1 (2010): 311-323. [21] Iwatsubo amyloid beta protein deposition 1994

[22] Selkoe, Dennis J. "Alzheimer's disease: genes, proteins, and therapy."*Physiological reviews* 81.2 (2001): 741-766.

[23] Tomaselli, Simona, et al. "The α-to-β Conformational Transition of Alzheimer's Aβ-(1–42) Peptide in Aqueous Media is Reversible: A Step by Step Conformational Analysis Suggests the Location of β Conformation Seeding."*ChemBioChem* 7.2 (2006): 257-267.

[24] Riek, Roland, et al. "NMR studies in aqueous solution fail to identify significant conformational differences between the monomeric forms of two Alzheimer peptides with widely different plaque-competence, Aβ (1–40) ox and Aβ (1–42) ox." *European Journal of Biochemistry* 268.22 (2001): 5930-5936.

[25] Shafrir, Yinon, et al. "Beta-barrel models of soluble amyloid beta oligomers and annular protofibrils." *Proteins: Structure, Function, and Bioinformatics* 78.16 (2010): 3458-3472.

[26] Stroud, James C., et al. "Toxic fibrillar oligomers of amyloid-β have cross-β structure." *Proceedings of the National Academy of Sciences* 109.20 (2012): 7717-7722.

[27] Balbach, John J., et al. "Supramolecular Structure in Full-Length Alzheimer's< i> β</i>-Amyloid Fibrils: Evidence for a Parallel< i> β</i>-Sheet Organization from Solid-State Nuclear Magnetic Resonance." *Biophysical journal* 83.2 (2002): 1205-1216.

[28] Ahmed, Mahiuddin, et al. "Structural conversion of neurotoxic amyloid-[beta] 1-42 oligomers to fibrils." *Nature structural & molecular biology* 17.5 (2010): 561-567.

[29] Matsuzaki, Katsumi. "Physicochemical interactions of amyloid β-peptide with lipid bilayers." *Biochimica et Biophysica Acta (BBA)-Biomembranes* 1768.8 (2007): 1935-1942.

[30] Terry, Robert D. "The pathogenesis of Alzheimer disease: an alternative to the amyloid hypothesis." *Journal of Neuropathology & Experimental Neurology*55.10 (1996): 1023-1025.

[31] Martins, Ivo Cristiano, et al. "Lipids revert inert Aβ amyloid fibrils to neurotoxic protofibrils that affect learning in mice." *The EMBO journal* 27.1 (2007): 224-233.

[32] Xue, Wei-Feng, et al. "Fibril fragmentation enhances amyloid cytotoxicity."*Journal of Biological Chemistry* 284.49 (2009): 34272-34282.

[33] Ryan, Timothy M., et al. "The Role of Aβ in Alzheimer's Disease." *Amyloid Fibrils and Prefibrillar Aggregates: Molecular and Biological Properties* (2013): 263-293.

[34] Shaw, David E., et al. "Millisecond-scale molecular dynamics simulations on Anton." *High Performance Computing Networking, Storage and Analysis, Proceedings of the Conference on*. IEEE, 2009.

[35] Kale, L., R. Skeel, M. Bhandarkar, R. Brunner, A. Gursoy, et al. 1999. NAMD2: greater scalability for parallel molecular dynamics. J. Com- put. Phys. 151:283–312.

[36] Miller, Yifat, Buyong Ma, and Ruth Nussinov. "Polymorphism of Alzheimer's Aβ17-42(p3) Oligomers: The Importance of the Turn Location and Its Conformation." *Biophysical journal* 97.4 (2009): 1168-1177.

[37] Sato T, Kienlen-Campard P, AhmedM, Liu W, Li H, et al. Inhibitors of amyloid toxicity based on beta-sheet packing of Abeta40 and Abeta42. Biochemistry 45: (2006) : 5503–5516.

[38] Sali, Andrej, and T. L. Blundell. "Comparative protein modelling by satisfaction of spatial restraints." *Protein structure by distance analysis* 64 (1994): C86.

[39] Humphrey, W., Dalke, A. and Schulten, K., "VMD - Visual Molecular Dynamics", J. Molec. Graphics, 1996, vol. 14, pp. 33-38.

[40] MacKerell, A. D., D. Bashford, M. Bellott, R. L. Dunbrack, J. D. Evan- seck, et al. 1998. All-atom empirical potential for molecular modeling and dynamics studies of proteins. J. Phys. Chem. B. 102:3586–3616.

[41] Brooks, B. R., R. E. Bruccoleri, B. D. Olafson, D. J. States, S. Swami- nathan, et al. 1983.CHARMM—a program for macromolecular energy, minimization, and dynamics calculations. J. Comput. Chem. 4:187–217.

[42] Lugli, F., Toschi, F., Biscarini, F., Zerbetto, F., & Ciamician, C. G. (2010). Electric Field Effects on Short Fibrils of A Amyloid Peptides, 3516–3526.

[43] Ryckaert, J.-P.; Ciccotti, G.; Berendsen, H. J. C. J. Comput. Chem. 1977, 23, 327–341.

[44] Mahoney, M. W., and W. L. Jorgensen. A five-site model for liquid water and the reproduction of the density anomaly by rigid, nonpolarizable potential functions. J. Chem. Phys. 112: 2000: 8910–8922.

[45] Jorgensen, W. L., J. Chandrasekhar, J. D. Madura, R. W. Impey, and M. L. Klein. Comparison of simple potential functions for simu- lating liquid water. J. Chem. Phys. 79: 1983: 926–935.

[46] Humphrey, W., Dalke, A. and Schulten, K., "VMD - Visual Molecular Dynamics", J. Molec. Graphics, 1996, vol. 14, pp. 33-38.

[47] Rubin, Noa, et al. "Chirality of amyloid suprastructures." *Journal of the American Chemical Society* 130.14 (2008): 4602-4603.

[48] Strodel, Birgit, et al. "Transmembrane structures for Alzheimer's Aβ1− 42 oligomers." *Journal of the American Chemical Society* 132.38 (2010): 13300-13312.

[49] Shafrir, Yinon, et al. "Models of membrane-bound Alzheimer's Abeta peptide assemblies." *Proteins: Structure, Function, and Bioinformatics* 78.16 (2010): 3473-3487. [50] Ma B., Nussinov R. J Biol Chem. 2010 November 19; 285(47): 37102–37110.

[51] Kahler, Anna, Heinrich Sticht, and Anselm HC Horn. "Conformational Stability of Fibrillar Amyloid-Beta Oligomers via Protofilament Pair Formation–A Systematic Computational Study." *PloS one* 8.7 (2013): e70521.

[52] Kahler et al.

[53] Ma, Buyong, and Ruth Nussinov. "Polymorphic C-terminal β-sheet interactions determine the formation of fibril or amyloid β-derived diffusible ligand-like globulomer for the Alzheimer Aβ42 dodecamer." *Journal of Biological Chemistry*285.47 (2010): 37102-37110.